environmental microbiology

Environmental Microbiology (2014) **16**(6), 1741–1754 doi:10.1111/1462-2920.12373

Toxin GhoT of the GhoT/GhoS toxin/antitoxin system damages the cell membrane to reduce adenosine triphosphate and to reduce growth under stress

Hsin-Yao Cheng,[1] Valerie W. C. Soo,[1] Sabina Islam,[1] Michael J. McAnulty,[1] Michael J. Benedik[3] and Thomas K. Wood[1,2]*

Departments of [1]Chemical Engineering and [2]Biochemistry and Molecular Biology, Pennsylvania State University, State College, PA 16802, [3]Department of Biology, Texas A & M University, College Station, TX 77843, USA.

Summary

Toxin/antitoxin (TA) systems perhaps enable cells to reduce their metabolism to weather environmental challenges although there is little evidence to support this hypothesis. *Escherichia coli* GhoT/GhoS is a TA system in which toxin GhoT expression is reduced by cleavage of its messenger RNA (mRNA) by antitoxin GhoS, and TA system MqsR/MqsA controls GhoT/GhoS through differential mRNA decay. However, the physiological role of GhoT has not been determined. We show here through transmission electron microscopy, confocal microscopy and fluorescent stains that GhoT reduces metabolism by damaging the membrane and that toxin MqsR (a 5′-GCU-specific endoribonuclease) causes membrane damage in a GhoT-dependent manner. This membrane damage results in reduced cellular levels of ATP and the disruption of proton motive force (PMF). Normally, GhoT is localized to the pole and does not cause cell lysis under physiological conditions. Introduction of an F38R substitution results in loss of GhoT toxicity, ghost cell production and membrane damage while retaining the pole localization. Also, deletion of *ghoST* or *ghoT* results in significantly greater initial growth in the presence of antimicrobials. Collectively, these results demonstrate that GhoT reduces metabolism by reducing ATP and PMF and that this reduction in metabolism is important for growth with various antimicrobials.

Received 28 October, 2013; revised 4 December, 2013; accepted 14 December, 2013. *For correspondence. E-mail tuw14@psu.edu; Tel. (+814) 863 4811; Fax (+814) 865 7846.

Introduction

In contrast to laboratory conditions, bacteria usually grow in close association (Kolter, 2010) and with nutritional limitations (Nguyen *et al.*, 2011); in fact, nutritional stress could be perceived as the universal stress (Khakimova *et al.*, 2013). Therefore, distinct mechanisms have evolved to acquire fitness advantages over competitors since resources are limited; for example, cells may activate cellular functions that are normally silent under laboratory conditions, such as the *bgl* operon in *Escherichia coli* for the uptake and metabolism of the β-glucosides salicin and arbutin (Prasad and Schaefler, 1974), or even kill competitors via bacteriocins. Furthermore, it has been hypothesized that cells may slow growth to acquire a competitive advantage; for example, to become more efficient in translation at times of reduced resources (Dethlefsen and Schmidt, 2007).

Bacteria can also weather unfavourable conditions by entering a dormant state known as the persister state where non-dividing cells can survive antibiotic treatments (Lewis, 2007). The most likely means for slowing growth during stress (in the extreme creating dormancy) is through toxin/antitoxin (TA) systems (Kim and Wood, 2010; Kwan *et al.*, 2013). TA systems are prevalent in free-living prokaryotes (at least 37 in *E. coli*) (Tan *et al.*, 2011), including many pathogenic bacteria (Gerdes *et al.*, 2005). Typically, a protein-based TA system consists of a stable toxin to disrupt cellular processes and an unstable antitoxin to counteract the effect of the toxin and to impose physiological regulation of the toxin activity (Jayaraman, 2008).

Besides dormancy, TA systems may play other important roles in cell physiology such as biofilm formation (Ren *et al.*, 2004; Kim *et al.*, 2008), phage inhibition (Pecota and Wood, 1996) and the general stress response (Wang and Wood, 2011; Wang *et al.*, 2011; Hu *et al.*, 2012). Toxins with their messenger RNA (mRNA) endoribonuclease activity activated by stress, such as MqsR and MazF, have a global impact on gene expression by enriching some transcripts, and thus they are becoming recognized as global regulators through this property of differential mRNA decay (Wang and Wood, 2011). In fact, the MqsR/MqsA TA system regulates

another TA system, GhoT/GhoS (Wang *et al*., 2013). Antitoxins such as MqsA and DinJ also have a global impact through their inhibition of stationary stress response sigma factor RpoS (Wang and Wood, 2011; Wang *et al*., 2011; Hu *et al*., 2012); this inhibition is relieved upon stress that results in antitoxin degradation.

Although TA systems are present in the bacterial genome, their impact on cell physiology is often not prominent, and there is usually no phenotype when a single system is deleted (Maisonneuve *et al*., 2011); however, an effect is usually observed with plasmid-based overexpression strategies or under various stress conditions. For example, several TA systems have been shown to be activated via amino acid or glucose starvation, including RelB/RelE (Christensen *et al*., 2001), HigB/HigA (Christensen-Dalsgaard and Gerdes, 2006) and YafN/YafO (Christensen-Dalsgaard *et al*., 2010); however, ectopic overexpression is usually required to exert their effect on bacterial growth. For the MazF/MazE TA system, an effect of *mazEF* deletion on bacterial growth is seen upon the introduction of severe environmental stresses, such as high temperature (50°C) and hydrogen peroxide (up to 50 mM) (Kolodkin-Gal and Engelberg-Kulka, 2006). Similarly, antibiotic stress (to create persister cells) is required to see the effect of the *mqsR* mutation (*mqsR* encodes toxin MqsR), and this was the first time the absence of a toxin was shown to affect persistence (Kim and Wood, 2010). Deletion of *tisB* encoding the toxin TisB of the TisB/IstR-1 TA system also reduces persistence (Dörr *et al*., 2010), but deletion of most toxin genes has no effect on persistence even with severe antibiotic stress (Keren *et al*., 2004).

Of the five types identified so far, TA systems have been classified as type I if the antitoxin RNA prevents the translation of toxin RNA, type II if the antitoxin protein binds and inhibits the toxin protein, and type III if the antitoxin RNA binds and inhibits the protein toxin (Hayes and Van Melderen, 2011). In the type IV TA system, the protein antitoxin interferes with binding of the toxin to its target rather than through a direct antitoxin/toxin binding (Masuda *et al*., 2012). In the recently identified type V TA system, the antitoxin GhoS is not labile during stress nor does it bind to DNA to regulate transcription; instead, it exhibits sequence-specific endoribonuclease activity to degrade *ghoT* mRNA, preventing its translation (Wang *et al*., 2012). Toxin GhoT in this system produces ghost cells when overproduced, but it has not been completely characterized in that it has not been shown to be a protein, it has not been determined whether it directly damages the membrane, nor has it been determined how it damages the membrane. We determine here the mechanism by which GhoT slows growth, by damaging the membrane at the cell poles, depleting cellular energy and disrupting the proton motive force (PMF). We also demonstrate that one physiological role of the GhoT/GhoS TA system is to reduce metabolism in the presence of several antimicrobials (carbenicillin, cefoxitin, 5,7-dichloro-8-hydroxyquinoline and 2-phenyphenol); hence, there is a distinct phenotype upon deletion of the *ghoST* locus.

Results

GhoT causes membrane damage

GhoT is predicted to be a small (57 aa), highly hydrophobic polypeptide and has been shown to cause cell lysis when overproduced (Wang *et al*., 2012). Here we used transmission electron microscopy (TEM) to confirm cellular membrane rupture upon GhoT overproduction. Three phenomena were observed for *E. coli* cells overexpressing GhoT (Fig. 1A, right): (i) nucleoid condensation and leakage into the extracellular space, (ii) enlargement of the periplasmic space and (iii) cell breakage. These observations are indicative of cell decay. As a negative control, cells producing GhoS (a cytoplasmic endoribonuclease) were examined, and no membrane damage was observed (Fig. 1A, left).

To investigate further how GhoT exerts its effect on the bacterial membrane, the cell morphology upon GhoT production was compared with the treatment of nisin, a channel-forming toxin that causes cell lysis (Lamsa *et al*., 2012), as well as the antibacterial compound carbonyl cyanide *m*-chlorophenyl hydrazine (CCCP), which disrupts membrane potential and ΔpH, the components of PMF (Liu *et al*., 2010). Because these compounds are normally only effective in Gram-positive bacteria (Lamsa *et al*., 2012), the *E. coli* strain NR698, deficient in *lptD* that encodes a protein required for outer membrane biogenesis, was utilized to assess the effect of the treatments (Sampson *et al*., 1989). As shown in Fig. 1B, no significant change in morphology was found for the negative control, NR698/pCA24N cells treated with dimethyl sulfoxide (DMSO), whereas cells producing GhoT (NR698/pCA24N-*ghoT*) showed signs of compromised membranes as evidenced by hyper-permeability to the nucleic acid stains, 4′,6-diamidino-2-phenylindole (DAPI) and SYTOX Green (Life Technologies, Grand Island, NY, USA; 42%, 63 out of ~150 cells counted). For the two positive controls, the cells became hyper-permeable when treated with nisin and had significant membrane damage when challenged with CCCP, as evidenced by faint FM4–64 signals, which was likely due to the inability of FM4–64 to bind to the highly compromised membranes.

Deletion of *ghoT* reduces the persistence of an MqsR-producing strain (Wang *et al*., 2012), and MqsR activates GhoT through differential mRNA decay (Wang *et al*., 2013). To see if MqsR production leads to membrane damage through GhoT, we compared the cell morphology of BW25113/pCA24N-*mqsR* and Δ*ghoT*/pCA24N-*mqsR*

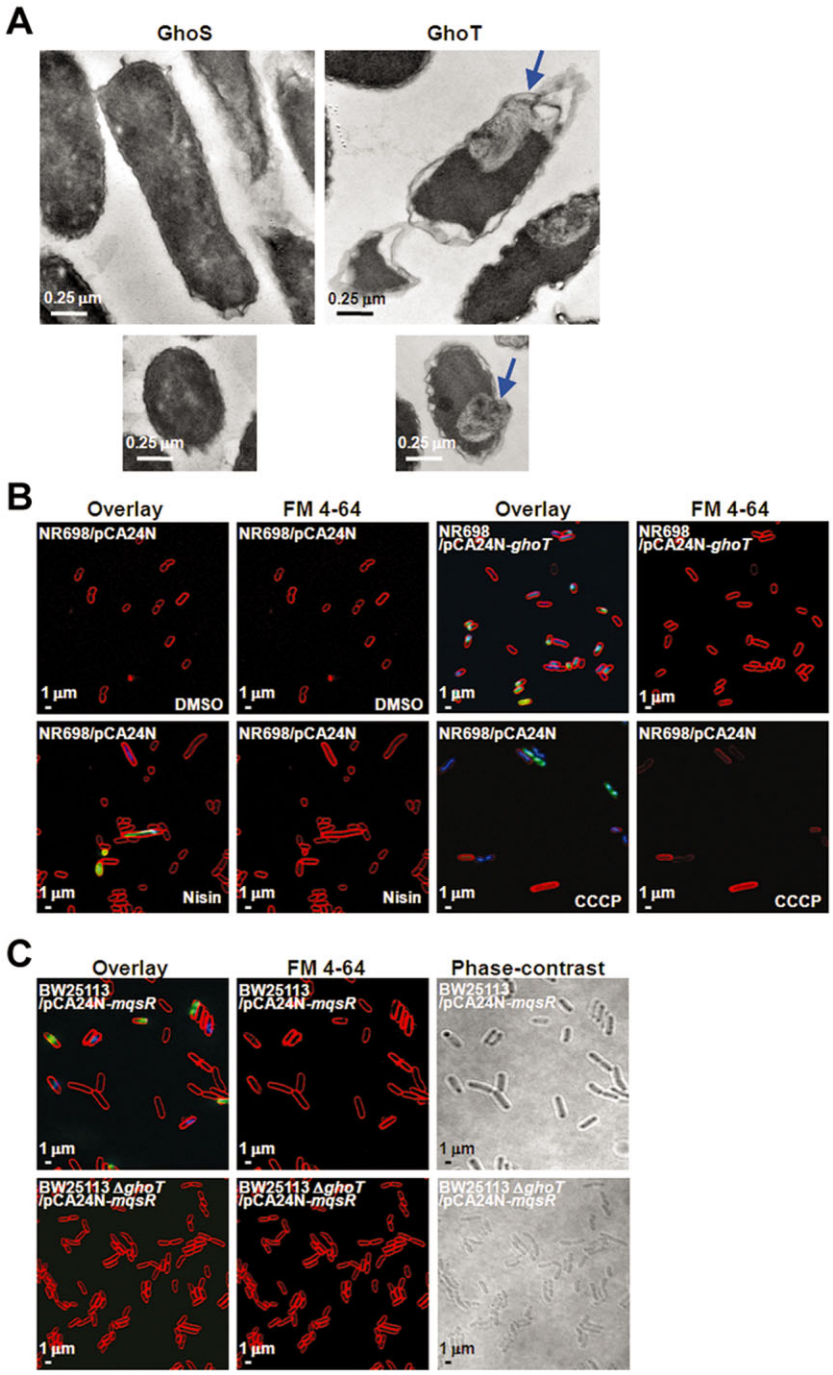

Fig. 1. GhoT production compromises the cell membrane, and MqsR-mediated membrane damage is GhoT-dependent.
A. TEM images of cells overproducing GhoS (left) and GhoT (right). The top two images represent longitudinal sections of a representative cell, while the bottom two images represent horizontal sections of a representative cell. Blue arrows point to leakage of nucleoid materials as a result of GhoT-mediated membrane damage. Scale bars represent 0.25 μm.
B. Membrane damage as visualized by fluorescence images of NR698/pCA24N cells treated with 0.5% DMSO, 10 μg ml^{-1} nisin and 500 μM CCCP for 1 h and of NR698/pCA24N-*ghoT* cells induced with 1 mM IPTG for 1 h.
C. Fluorescence images of BW25113/pCA24N-*mqsR* or Δ*ghoT*/pCA24N-*mqsR* cells induced with 1 mM IPTG for 1 h. The overlay (FM 4–64, DAPI and SYTOX Green), FM 4–64 only and the phase-contrast microscope images are shown. Scale bars represent 1 μm.

with isopropyl β-D-1-thiogalactopyranoside (IPTG) induction. As shown in Fig. 1C, a portion of cells producing MqsR became hyper-permeable to the nucleic acid stains (13%, 200 out of ~1500 cells counted) and showed condensed poles characteristic of ghost cells; in contrast, this was not observed in the Δ*ghoT* mutant (0.3% compromised cells, 8 out of ~2600 cells counted). The results show that the production of the 5′-GCU-specific RNase MqsR causes membrane damage in a GhoT-dependent manner, supporting our previous conclusion that the type II TA MqsR/MqsA controls the type V TA GhoT/GhoS (Wang *et al.*, 2013).

GhoT does not lyse cells under physiological conditions

Because it was unclear whether GhoT causes membrane damage and cell lysis without ectopic expression, we first investigated membrane integrity by microscopic analysis of BW25113 and the Δ*ghoT* mutant grown in M9-Glu

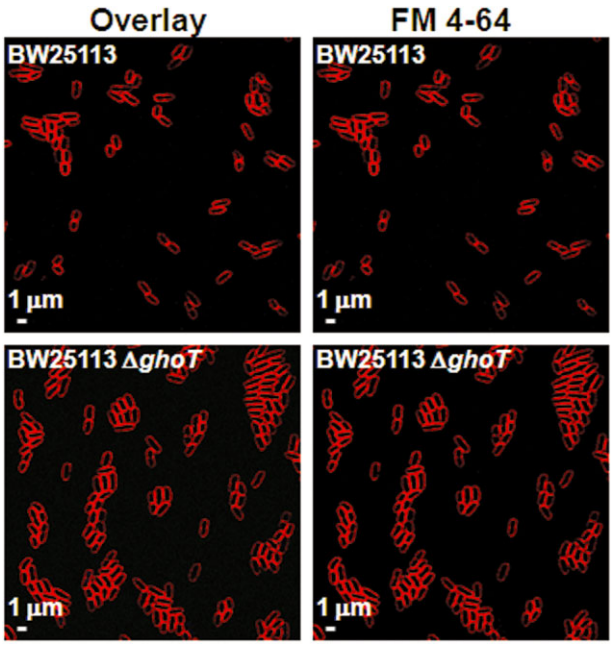

Fig. 2. GhoT does not cause cell damage without ectopic expression. Fluorescence images of the wild-type (BW25113) and Δ*ghoT* mutant grown in M9-Glu medium for 8 h. The overlay (FM 4–64, DAPI and SYTOX Green) and FM 4–64 only images are shown. Scale bars represent 1 μm.

medium (turbidity of 0.8 to 1.0) (Fig. 2); for BW25113, 0 out of ~500 cells showed a compromised membrane, and for the Δ*ghoT* mutant, 0 out of ~1200 cells showed a compromised membrane. To provide a more quantitative comparison, cell lysis was investigated by determining the extent to which β-galactosidase is released into the supernatant compared to intracellular β-galactosidase. During exponential growth in M9-Glu medium, we did not observe significant cell lysis upon deleting *ghoT*: for BW25113/pCA24N-*lacZ*, there was 0.018 ± 0.006% lysis, and for Δ*ghoT*/pCA24N-*lacZ*, there was 0.022 ± 0.014% lysis. Similarly, during nutrient starvation imposed by overnight growth in M9-Glu medium, we did not observe significant cell lysis using the β-galactosidase assay (0.096 ± 0.042% for BW25113 versus 0.05 ± 0.01% for the Δ*ghoT* mutant). As a control, we observed 5.4 ± 0.6-fold more cell lysis from GhoT overproduction (MG1655/pCA24N-*ghoT* versus MG1655/pCA24N). Therefore, together, our results suggest that, without ectopic expression, GhoT does not cause cell lysis.

GhoT functions as a protein and Phe38 is important for its toxicity

The toxin MqsR cleaves *ghoS* mRNA preferentially over *ghoT* mRNA *in vitro* and *in vivo*, which likely increases the relative level of free GhoT (Wang *et al*., 2013). Although the *ghoT* transcript does not harbour 5′-GCU, the primary MqsR cleavage recognition site (Yamaguchi *et al*., 2009), the transcript contains three of the less favourable 5′-GCA recognition sites. To investigate if any of these sites would affect GhoT toxicity *in vivo*, we introduced nucleotide substitutions to alter each of these 5′-GCA sites without changing the encoded amino acids. Three plasmids were generated: pCA24N-*ghoT*GCA1 with GC*A* (Ala) changed to GC*C* (Ala) at aa position 2, pCA24N-*ghoT*GCA2 with GC*A* (Ala) changed to GC*C* (Ala) at aa position 37, and pCA24N-*ghoT*GCA3 with GC*A* (Ala) changed to GC*C* (Ala) at aa position 51. In addition, to confirm that GhoT functions as a protein, mutations were introduced to pCA24N-*ghoT* to generate plasmid pCA24N-*ghoT*ATG, which harbours a nucleotide substitution where A*T*G (Met) was changed to A*C*G (Thr) at GhoT aa position 1. Toxicity was then determined with a Δ*ghoS* mutant carrying each pCA24N derivative, grown on IPTG-containing media. As shown in Fig. 3A, Δ*ghoS*/pCA24N-*ghoT* did not grow on IPTG-containing media; however, Δ*ghoS*/pCA24N-*ghoT*ATG grew normally, showing that GhoT is a toxic protein because the removal of its start codon abolished toxicity. In addition, the MqsR secondary recognition 5′-GCA sites in *ghoT* are not important for toxicity because none of the Δ*ghoS* strains harbouring pCA24N derivatives with mutated 5′-GCA sites had enhanced GhoT toxicity on IPTG-containing media. Hence, *ghoT* mRNA does not appear to be processed by MqsR *in vivo*.

To identify residues important for GhoT activity, we modelled the GhoT structure using PHYRE2 (Kelley and Sternberg, 2009). The modelled GhoT monomeric structure harbours two helices that appear to be transmembrane spanning regions (Fig. 3C). The termini of both transmembrane helices appear to be stabilized by a putative hydrophobic interaction formed between Ile21 and Phe38 at close proximity (interatomic distance less than 3 Å). To investigate if either of these residues helps stabilize GhoT in the inner membrane to confer its toxicity, we disrupted this hydrophobic interaction by separately changing Ile21 and Phe38 to Arg, with a bulky positively charged side chain, via plasmids pCA24N-*ghoT*I21R and pCA24N-*ghoT*F38R respectively. As shown in Fig. 3B and D, Δ*ghoS* carrying pCA24N, pCA24N-*ghoS* and pCA24N-*ghoT*F38R grew normally with IPTG induction in both solid and liquid media, while the strains producing GhoT and GhoTI21R were unable to grow.

Because overproduction of GhoT led to cell lysis (Wang *et al*., 2012), which caused complications in detection of the recombinant protein, the loss of toxicity of GhoTF38R provided a chance to detect and identify its cellular localization. As expected, GhoTF38R was detected in the initial cell pellet and in the membrane fraction via Western

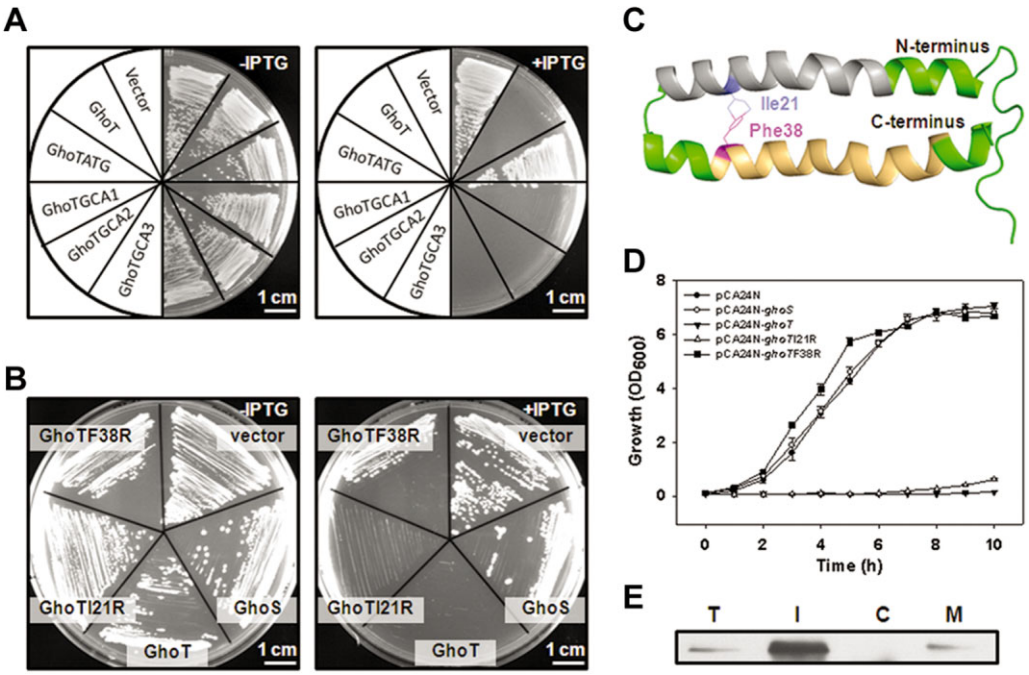

Fig. 3. GhoT is a toxic protein and the F38R substitution inactivates GhoT.
A and B. Growth of Δ*ghoS* transformants carrying pCA24N derivatives with *ghoT* mutations on LB plates with kanamycin (50 μg ml^{-1}) and chloramphenicol (30 μg ml^{-1}) without or with 1 mM IPTG. Vector, pCA24N; GhoT, pCA24N-*ghoT*; GhoTATG, pCA24N-*ghoT*ATG encoding GhoT with the start codon changed to Thr; GhoTGCA1, pCA24N-*ghoT*GCA1 encoding a silent change of the MqsR secondary cleavage site to GCC; GhoTGCA2, pCA24N-*ghoT*GCA2 encoding a silent change of the MqsR secondary cleavage site to GCC; GhoTGCA3, pCA24N-*ghoT*GCA3 encoding a silent change of the MqsR secondary cleavage site to GCC; GhoS, pCA24N-*ghoS*; GhoTI21R, pCA24N-*ghoT*I21R encoding GhoT with the I21R substitution; GhoTF38R, pCA24N-*ghoT*F38R encoding GhoT with the F38R substitution. Three independent cultures were evaluated. Scale bars represent 1 cm.
C. GhoT structure modelled by PHYRE2 (Kelley and Sternberg, 2009). Transmembrane spanning regions are annotated by UniProt (The UniProt Consortium, 2012) and are shown as gray and orange regions. The predicted positions of Ile21 and Phe38 are indicated.
D. Growth of cells carrying different plasmids in LB medium with chloramphenicol (30 μg ml^{-1}) and 1 mM IPTG. Three independent cultures were evaluated. Error bars, s.e.m. ($n = 3$).
E. Western blot analysis of GhoTF38R. T, IPTG-induced total intracellular cell protein; I, insoluble fraction after ultracentrifugation and extraction with 6 N urea; C, cytoplasmic fraction after ultracentrifugation and extraction with 6 N urea; M, membrane fraction after ultracentrifugation.

blot analysis after ultracentrifugation (Fig. 3E); under the same conditions, native GhoT was not detected. Collectively, the results suggest that Phe38 is important for GhoT toxicity, and GhoT is a membrane protein.

GhoT localizes at the cell pole

To investigate the cellular localization of GhoT, we examined BW25113 producing GhoT with a GFP fusion (via pCA24N-*ghoT*GFP) using confocal microscopy and determined that GhoT-GFP proteins localize at the poles (Fig. 4A, upper panel). In order to verify if the loss of toxicity with GhoTF38R was due to altered cellular localization, the plasmid pCA24N-*ghoT*F38RGFP was constructed, and we determined that GhoTF38R-GFP also localizes at the poles (Fig. 4A, lower panel). Using nucleic acid stains, DAPI and SYTOX Green, we compared the membrane damage caused by overproduction of wild-type GhoT and GhoTF38R. We found that GhoT producing cells became more permeable (61%, 76 out of 124 cells became permeable) (Fig. 4B, overlay, upper panel) while most of the GhoTF38R producing cells remained intact (3.52%, 60 out of ~1700 cells became permeable) (Fig. 4B, overlay, lower panel). In addition, using phase-contrast microscopy, we found that overproduction of GhoTF38R reduced ghost cell formation compared with native GhoT production (Fig. 4B, phase-contrast). The polar localization of GhoT was not due to the accumulation of cellular proteins at the poles (which is the outcome of ghost cell formation) as we observed an even distribution of GFP in the control experiment in which cells produced GhoT and GFP separately (Fig. 4C). These results demonstrate that GhoT is a pole-localized protein and that introduction of the F38R substitution to GhoT renders it unable to cause membrane damage while maintaining the pole localization.

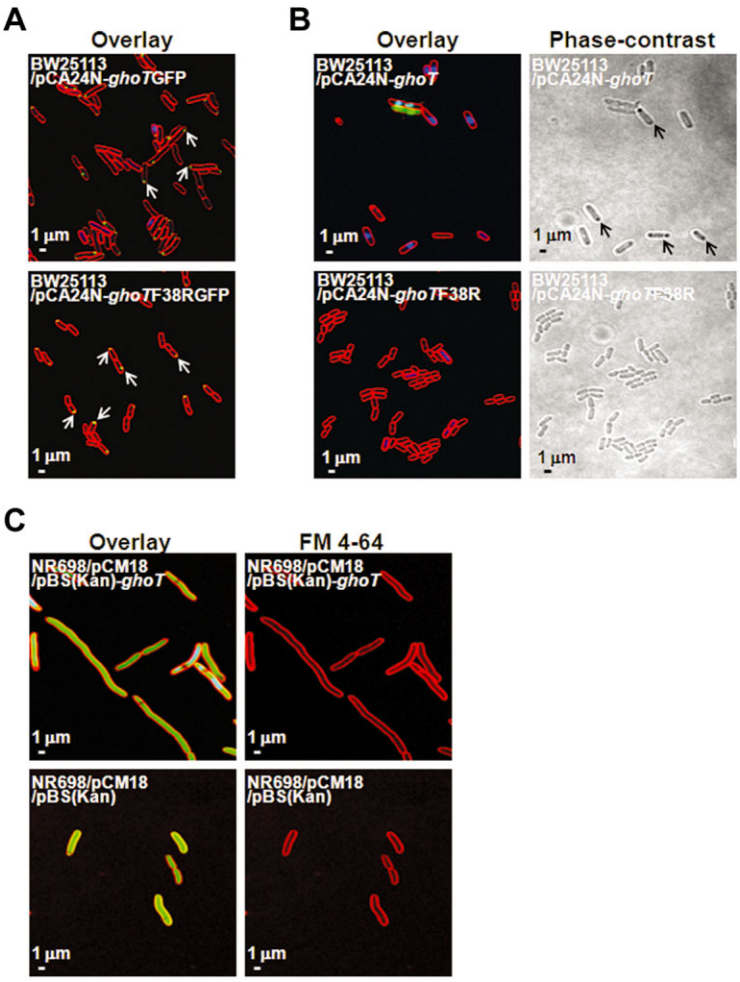

Fig. 4. GhoT localizes to the poles and substitution F38R reduces cell membrane damage and ghost cell formation.
A. Fluorescence images of BW25113/pCA24N-*ghoT*GFP and BW25113/pCA24N-*ghoT*F38RGFP showing GhoT localizes at the pole. Cells were grown in LB with chloramphenicol (30 μg ml^{-1}) and induced with 1 mM IPTG for 1 h. The white arrows indicate polar GFP proteins produced in the cells.
B. Membrane damage as visualized by fluorescence images of BW25113/pCA24N-*ghoT* and BW25113/pCA24N-*ghoT*F38R grown in LB with chloramphenicol (30 μg ml^{-1}) and induced with 1 mM IPTG for 1 h. The overlay (FM 4–64, DAPI and SYTOX Green) and the phase-contrast microscope images are shown. The black arrows indicate ghost cells.
C. Fluorescence images of *E. coli* NR698 transformants carrying pCM18 (producing GFP) and pBS(Kan) or pCM18 and pBS(Kan)-*ghoT* (producing GhoT) grown with IPTG induction (1 mM for 1 h). Samples were stained with FM4–64 and DAPI. The overlay (FM 4–64 and DAPI) and FM 4–64 images are shown. Scale bars represent 1 μm.

GhoT reduces intracellular ATP levels and dissipates PMF

Because GhoT overproduction compromises membrane integrity, we hypothesized that the PMF would be disrupted, and subsequently the ATP concentration would be reduced from the leakage of nucleotides. To investigate the intracellular ATP concentrations quantitatively, a luciferase-based assay was performed using cell extracts prepared from IPTG-induced cultures. As shown in Fig. 5A, an 88-fold reduction in cellular ATP was found in BW25113/pCA24N-*ghoT* cells compared with BW25113/pCA24N after 1 mM IPTG induction for 2 h. In contrast, overproduction of GhoTF38R did not reduce intracellular ATP significantly (1.8-fold reduction compared with BW25113/pCA24N). Therefore, GhoT production depletes the cellular pool of ATP.

If GhoT disrupts PMF, it is expected that a portion of the cells should become polarized or depolarized because they have lost the ability to maintain the membrane potential. Hence, we used flow cytometry to detect the fluorescence released by $DiBAC_4(3)$, a potential sensitive dye that enters depolarized cells and binds to membranes and proteins (Berney *et al.*, 2006). As negative controls, NR698/pCA24N (with a compromised outer membrane) and BW25113/pCA24N cells were treated with DMSO, and for a positive control, cells were treated with CCCP (Wu *et al.*, 2010). As shown in Fig. 5B, CCCP treatment rendered NR698/pCA24N highly depolarized, as reflected by the increased fluorescence signal, compared with the strain treated with 0.5% DMSO. The effect of CCCP on BW25113/pCA24N cells was less pronounced, probably because of its intact outer membrane structure. However, both BW25113/pCA24N-*ghoT* and NR698/pCA24N-*ghoT* cells became highly depolarized with IPTG induction (Fig. 5C). The effect of GhoT production in BW25113 cells was not as pronounced because not all the cells became depolarized as seen with NR698/pCA24N-*ghoT* cells. The membrane potential in both hosts remained unaffected with GhoTF38R overproduction because no significant increase in the fluorescence signal was observed. These results show that GhoT accumulation either depletes or

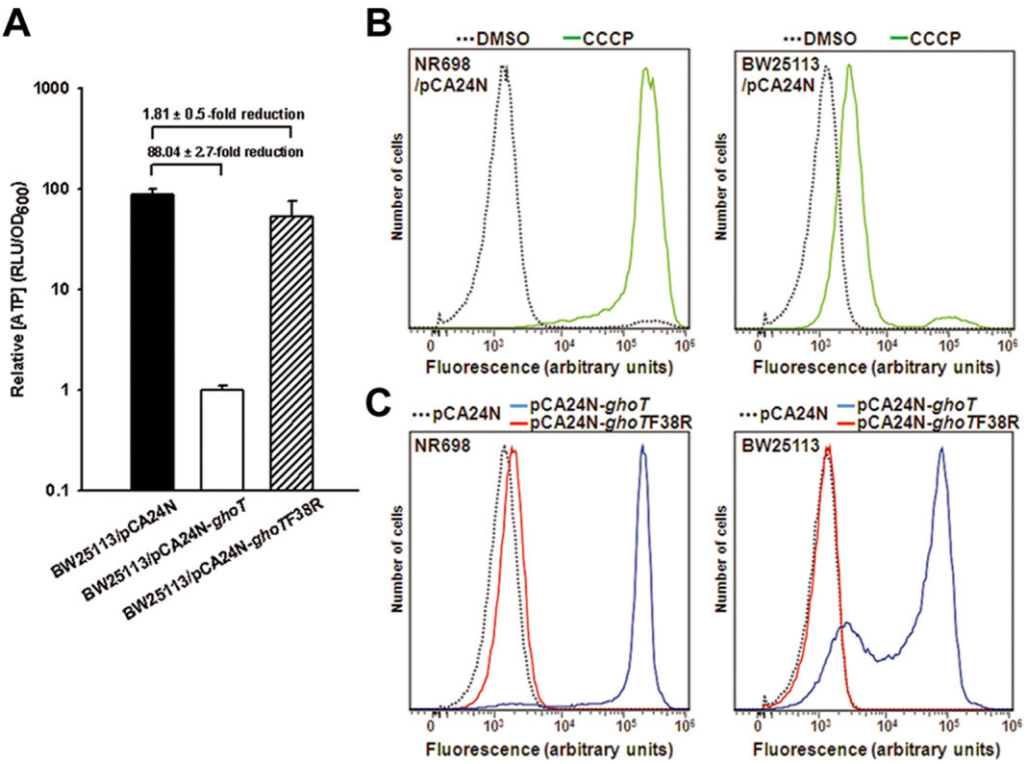

Fig. 5. GhoT reduces intracellular ATP levels and disrupts the membrane potential.
A. Nucleotides from cultures induced with 1 mM IPTG for 2 h were extracted by TCA, and a luciferase-based assay was performed to determine ATP concentrations. The ATP levels were expressed as RLU/OD_{600} (relative light units/optical density at 600 nm). The fold reduction relative to the vector control strain is indicated. Representative results from two of the three independent trials are shown and depicted as the average ± standard deviation.
B. Flow cytometry assay using $DiBAC_4(3)$ stained NR698/pCA24N (left) or BW25113/pCA24N (right) treated with 0.05% DMSO (black, dotted line, negative control) or 500 μM CCCP (green) for 1 h. Two independent cultures were evaluated.
C. Flow cytometry assay using $DiBAC_4(3)$ stained NR698 (left) or BW25113 (right) carrying pCA24N (black, dotted line), pCA24N-*ghoT* (blue) or pCA24N-*ghoT*F38R (red) induced with 1 mM IPTG for 1 h. Two independent cultures were evaluated.

leaks cellular ATP, that GhoT dissipates the membrane potential and that the F38R substitution abolishes these toxic effects.

GhoT/GhoS protect the cell from antimicrobials

To ascertain the physiological importance of the GhoT/GhoS TA locus, we conducted phenotype arrays to simultaneously test 1920 different growth conditions for the wild-type versus the Δ*ghoST* ΔKan mutant. Note that it was imperative to utilize the scarless mutant (i.e. no antibiotic marker) so that the only genotypic difference was the deletion of the *ghoST* locus to avoid studying an effect that is an artifact of a residual antibiotic marker. These battery of tests investigate differences in metabolism between the two strains for basic cellular nutritional pathways (i.e. for C, N, P and S metabolism), for osmotic and pH sensitivity and for sensitivity to chemical agents. The measured metabolism assays cell respiration (reduced nicotinamide adenine dinucleotide production) through a redox indicator (Bochner *et al.*, 2001): as the cells respire, a tetrazolium dye is reduced to formazan to form a strong purple colour so more colour indicates more rapid metabolism. No differences were found for the nutritional pathways and for osmotic and pH sensitivity; however, the Δ*ghoST* ΔKan mutant had more metabolism with four antimicrobials (carbenicillin, cefoxitin, 5,7-dichloro-8-hydroxyquinoline and 2-phenyphenol) (Fig. 6A). 5,7-dichloro-8-hydroxyquinoline is an antibacterial drug used in infectious diarrhoea, 2-phenylphenol is a general disinfectant, cefoxitin is a second-generation cephalosporin that inhibits cell wall synthesis and carbenicillin is a bacteriolytic antibiotic similar to penicillin.

We then focused on carbenicillin and cefoxitin and found that the Δ*ghoST* ΔKan mutant consistently had more metabolism initially with carbenicillin (3.5 μg ml^{-1}) and cefoxitin (2.0 μg ml^{-1}), but the wild-type strain ultimately achieved greater metabolism (Fig. 6B). Similarly, the Δ*ghoT* ΔKan mutant had as much as 86 ± 1-fold faster

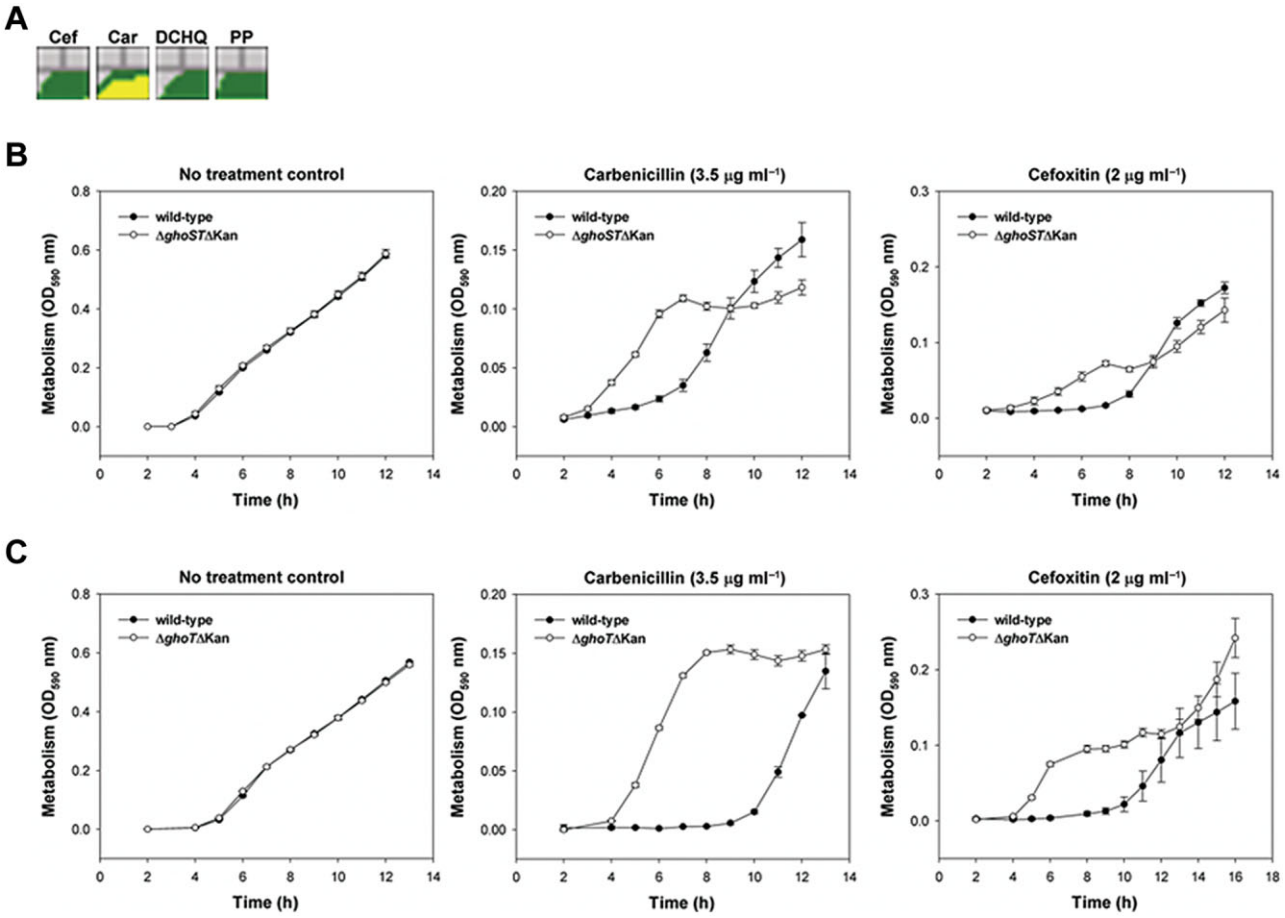

Fig. 6. GhoT/GhoS reduces cellular metabolisms under antimicrobial stress.
A. Initial results from BioLog phenotype microarray (PM) showing higher metabolic activity in the Δ*ghoST* ΔKan mutant (green) compared with the wild-type strain (yellow) in response to cefoxitin (Cef, well E4 in plate PM14), carbenicillin (Car, well G5 in plate PM14), 5,7-dichloro-8-hydroxyquinoline (DCHQ, well C3 in PM15) and 2-phenyphenol (PP, well H8 in PM18). The metabolic activity (y axis) for each strain was monitored for 48 h (*x*-axis). The consensus results from two independent trials are shown. Comparison of metabolic activities between (B) the wild-type and Δ*ghoST* ΔKan mutant and between (C) the wild-type and the Δ*ghoT* ΔKan mutant, in the presence of carbenicillin (3.5 μg ml^{-1}) and cefoxitin (2.0 μg ml^{-1}). Six independent colonies of each strain were evaluated in separate trials which yielded similar results (representative values are shown from two independent colonies from one trial), and the error bars represent standard deviations.

metabolism at 6 h with carbenicillin (Fig. 6C) and 21 ± 7-fold faster metabolism at 6 h with cefoxitin; however, the Δ*ghoT* ΔKan mutant always had greater metabolism than the wild type in the presence of these two antibiotics, which indicates that the antitoxin is required to regulate the toxin to slow the cellular metabolism, which is sometimes beneficial (e.g. persister cell formation). Critically, there was no difference in metabolism at all times in the absence of stress, so the strains were inoculated with the same number of active cells and grew identically (Fig. 6B and C, first panels). Although speculative, our results also suggest that under stressful conditions, while the toxin GhoT suppresses bacterial growth at the initial stage, the antitoxin GhoS eventually counteracts the effect to confer greater growth in the wild-type system. Therefore, the GhoT/GhoS locus is used by the cell to fine-tune growth during stress.

Discussion

In this study, we demonstrate that GhoT is responsible for causing membrane damage upon MqsR-producing conditions, which is crucial for cells to enter the dormant state to become persisters. GhoT acts as a pole-localized membrane toxin that reduces cellular metabolism by causing membrane damage, by reducing cellular ATP levels and by disrupting membrane potential. Collectively, we determine how GhoT slows cell growth and then show that this reduction in metabolism is important for growth in the presence of several antimicrobials under physiological conditions.

To date, the phenomenon of bacterial programmed cell death (PCD) is based on the study of the *E. coli* MazF/MazE TA system in which toxin MazF performs the dual role of either reversible stasis or cell death (Amitai *et al.*,

2009). MazF/MazE triggers cell death in response to culture density; i.e. MazF/MazE-mediated death is population dependent so that the death of the bulk cell population provides nutrients for survivor cells to resume growth as the conditions become propitious (Engelberg-Kulka *et al*., 2006). Compared with the MazF/MazE system, GhoT/GhoS-mediated metabolic slowdown is distinct from bacterial PCD in that there were no significant signs of cell lysis from activation of chromosomal GhoT; in addition, the reduced growth under stress conditions is likely the outcome of energy depletion from continuous membrane damage by GhoT.

Similar to the SOS-induced inner membrane toxin TisB (Unoson and Wagner, 2008), GhoT damages the inner membrane and reduces ATP production and reduces the PMF. The cause of the loss of toxicity for GhoTF38R remains to be discerned. In the absence of empirical structural data, we assumed that F38R and I21R would yield non-toxic GhoT, as the charged arginines would damage the putative interaction held by Phe38 and Ile21. This subsequently perhaps creates a structural bottleneck where either GhoT oligomerization, interaction with other binding partners or its insertion into cell membrane is disrupted. However, we propose that Phe38 has a functional role instead of a structural role, based on two lines of evidence: (i) in contrast to GhoTF38R, GhoTI21R is toxic (Fig 3B and D); and (ii) similar to GhoT, GhoTF38R remains localized at the cell poles (Fig 4A and B). Therefore, the non-toxicity of GhoTF38R appears to be due to the mutation itself, rather than a failure in oligomerization, abolished interaction or membrane insertion. We further speculate that Phe38 might form a 'phenylalanine clamp' that aligns the polypeptide in pores formed by GhoT oligomers. For example, a ring of seven phenylalanines forms a hydrophobic core in the anthrax toxin, and substrate recognition is facilitated by hydrophobic effect, π-π interaction and cation-π interaction (Krantz *et al*., 2005; Janowiak *et al*., 2010). By analogy, the charged arginines in GhoTF38R may 'seal off' the pores and, thus, limit leakage of cellular materials to the outer environment. Our results from confocal microscopy, the ATP assay and PMF flow cytometry support the notion that material leakage is minimal in GhoTF38R-expressing cells.

Protein localization has several important impacts on cell physiology, including chemotaxis (Sourjik and Berg, 2000), osmoregulation (Romantsov *et al*., 2007), cell division (Wu and Errington, 2003), phage attack (Edgar *et al*., 2008) and elimination of non-functional protein aggregates (Winkler *et al*., 2010). The pole localization of GhoT-GFP and GhoTF38R-GFP (Fig. 4) provides indirect evidence for the production of both proteins, and to our knowledge, this is the first demonstration of cellular localization of a bacterial toxin of a TA pair (here, at the poles). It is currently unknown, though, if such pole localization is regulated by cellular systems such as MinCDE, which oscillate from pole to pole to ensure the assembly of the FtsZ pre-division ring at mid-cell (Li and Young, 2012).

Protein aggregation resulting from failure of quality control is not uncommon under stressful conditions. In *E. coli*, these aggregates are known to be delivered to the poles to form a large polar aggregate (LPA), and the formation, delivery and disaggregation of LPA are all energy dependent (Rokney *et al*., 2009). This implies that the disruption of PMF and the reduction of ATP levels by GhoT production may have a negative effect on breaking down the aggregated proteins at the poles. Based on this assumption, it can also be inferred that the striking GhoT-induced ghost cell phenotype may be the result of LPA formation at the poles while GhoT may exert its effect through a global impact on energy supply or through a direct interaction with chaperone proteins (such as DnaK and DnaJ) or proteases (such as ClpB) to prevent the removal of LPAs. The latter hypothesis is supported by the result that GhoT localizes at the poles (Fig. 4) and that these proteins are recruited to the poles to dissolve LPAs in conjunction (Acebrón *et al*., 2008; Doyle and Wickner, 2009). It should be noted that GhoTF38R, which is non-toxic, also localizes at the poles; therefore, it is also likely that the F38R substitution abolishes the interaction between GhoT and its partners, if any.

It was hypothesized that lower levels of GhoT increases bacterial persistence by inducing a dormant state while the cell lysis is an ultimate outcome of overexpression (Wang *et al*., 2012). Here we show that cell lysis does not occur without ectopic expression of *ghoT* (Fig. 2), and thus GhoT does not seem to play a role in releasing cellular components, such as DNA or nutrients, for the rest of the population under physiological conditions. Therefore, when GhoT is active, the majority of cells have reduced metabolism; however, for those cells in which GhoT is overproduced as a result of normal fluctuations in protein activity for individual cells, they suffer severe energy depletion and become persister cells (dormant).

Although the exact mechanism of how GhoT damages the membrane remains to be elucidated, it is clear that one of the physiological roles of this bacterial TA system is a component of the stress response. Because the GhoT/GhoS TA system significantly decreases growth in the presence of four antimicrobials with diverse bacterial modes of action (e.g. cell wall synthesis, disinfectant and bacteriostatic agent), this TA system plays an integral part in adaptation of growth under unfavourable conditions. Also, it appears that the cell chooses to reduce metabolic activity (i.e. to keep the TA system) so ultimately it achieves greater metabolism during stress. Therefore, these results serve to cement the importance of TA systems for growth under stress.

Table 1. Bacterial strains and plasmids used in this study. The antibiotics used are ampicillin (100 μg ml^{-1}), chloramphenicol (30 μg ml^{-1}), erythromycin (300 μg ml^{-1}) and kanamycin (50 μg ml^{-1}).

Bacterial strains/plasmids		
E. coli K12 strains		Source
TG1	*supE thi-1* Δ*(lac-proAB)* Δ*(mcrB-hsdSM)5, (r_K^- m_K^-)*, F′ [*traD36 proAB*$^+$ *lacI*^{q} *lacZ*ΔM15]	Stratagene
NR698	MC4100 *lptD4213*	Ruiz and colleagues (2005)
MG1655	F$^-$ λ$^-$ *ilvG*$^-$ *rfb*-50 *rph*-1	Blattner and colleagues (1997)
BW25113	*lacI*^{q}*rrnB*$_{T14}$Δ*lacZ*$_{WJ16}$ *hsdR514*Δ*araBAD*$_{AH33}$Δ*rhaBAD*$_{LD78}$	Baba and colleagues (2006)
BW25113 Δ*ghoT*	BW25113 Δ*ghoT* Ω Km^R	Baba and colleagues (2006)
BW25113 Δ*ghoS*	BW25113 Δ*ghoS* Ω Km^R	Baba and colleagues (2006)
BW25113 Δ*ghoST*	BW25113 Δ*ghoST* Ω Km^R	This study
BW25113 Δ*ghoT* ΔKan	BW25113 Δ*ghoT*	This study
BW25113 Δ*ghoST* ΔKan	BW25113 Δ*ghoST*	This study
Plasmids		
pCA24N	Cm^R; *lacI*^{q}	Kitagawa and colleagues (2005)
pCA24N-*lacZ*	Cm^R; *lacI*^{q} P$_{T5\text{-}lac}$::*lacZ*$^+$	Kitagawa and colleagues (2005)
pCA24N-*mqsR*	Cm^R; *lacI*^{q} P$_{T5\text{-}lac}$::*mqsR*$^+$	Kitagawa and colleagues (2005)
pCA24N-*ghoS*	Cm^R; *lacI*^{q} P$_{T5\text{-}lac}$::*ghoS*$^+$	Kitagawa and colleagues (2005)
pCA24N-*ghoT*	Cm^R; *lacI*^{q} P$_{T5\text{-}lac}$::*ghoT*$^+$	Kitagawa and colleagues (2005)
pCA24N-*ghoT*ATG	Cm^R; *lacI*^{q} P$_{T5\text{-}lac}$::*ghoT*$^+$ with start codon replaced with ACG	This study
pCA24N-*ghoT*GCA1	Cm^R; *lacI*^{q} P$_{T5\text{-}lac}$::*ghoT*$^+$ with altered sequence GCA to GCC at nucleotide position 54 relative to the 6xHis-GhoT start codon	This study
pCA24N-*ghoT*GCA2	Cm^R; *lacI*^{q} P$_{T5\text{-}lac}$::*ghoT*$^+$ with altered sequence GCA to GCC at nucleotide position 159 relative to the 6xHis-GhoT start codon	This study
pCA24N-*ghoT*GCA3	Cm^R; *lacI*^{q} P$_{T5\text{-}lac}$::*ghoT*$^+$ with altered sequence GCA to GCC at nucleotide position 201 relative to the 6xHis-GhoT start codon	This study
pCA24N-*ghoT*I21R	Cm^R; *lacI*^{q} P$_{T5\text{-}lac}$::*ghoT*$^+$ with altered sequence TT to GA at nucleotide position 110-111 relative to the 6xHis-GhoT start codon	This study
pCA24N-*ghoT*F38R	Cm^R; *lacI*^{q} P$_{T5\text{-}lac}$::*ghoT*$^+$ with altered sequence TT to CG at nucleotide position 160-161 relative to the 6xHis-GhoT start codon	This study
pCA24N-*ghoT*GFP	Cm^R; *lacI*^{q} P$_{T5\text{-}lac}$::*ghoT-gfp*$^+$	Kitagawa and colleagues (2005)
pCA24N-*ghoT*F38RGFP	Cm^R; *lacI*^{q} P$_{T5\text{-}lac}$::*ghoT*F38R-*gfp*$^+$	This study
pBS(Kan)	Km^R	Canada and colleagues (2002)
pBS(Kan)-ghoT	Km^R P$_{lac}$::*ghoT*$^+$	Wang and colleagues (2012)
pCM18	Em^R; pTRKL2-P$_{CP25}$-RBSII-*gfp*mut3*-T$_0$-T$_1$	Hansen and colleagues (2001)
pCP20	Ap^R; Cm^R, *FLP*$^+$, λ *c*I857$^+$, λ p_RRep^{ts}	Datsenko and Wanner (2000)

Ap^R, Cm^R, Km^R and Em^R are ampicillin, chloramphenicol, kanamycin and erythromycin resistance respectively.

Experimental procedures

Bacterial strains, plasmids and growth conditions

Bacterial strains and plasmids used are listed in Table 1. Experiments were conducted at 37°C in Luria-Bertani (LB) medium unless indicated otherwise. The Δ*ghoST* mutant strain was constructed via the λ Red method (Datsenko and Wanner, 2000) using polymerase chain reaction (PCR) primers D*ghoST*fwd and D*ghoST*rev (Table 2) and verified by PCR using primers C*ghoST*fwd2 and C*ghoST*rev2 (Table 2) as well as by sequencing. The kanamycin resistance cassette was removed from Δ*ghoST* and Δ*ghoT* using pCP20 (Datsenko and Wanner, 2000), and verified by PCR using primers C*ghoST*fwd2 and C*ghoST*rev2 (Table 2) and by sequencing.

Site-directed mutagenesis

PCR was performed using pCA24N-*ghoT* or pCA24N-*ghoT*GFP (Table 1) as the template with different sets of primers (Table 2). The PCR products were recovered, subjected to *Dpn*I digestion and transformed into *E. coli* TG1 (Table 1). The plasmids prepared from the resulting transformants were confirmed by sequencing and designated as pCA24N-*ghoT*ATG, pCA24N-*ghoT*GCA1, pCA24N-*ghoT*GCA2, pCA24N-*ghoT*GCA3, pCA24N-*ghoT*I21R, pCA24N-*ghoT*F38R and pCA24N-*ghoT*F38RGFP (Table 1).

TEM

BW25113/pCA24N-*ghoS* and BW25113/pCA24N-*ghoT* were grown in LB-chloramphenicol to a turbidity at 600 nm of 0.5, and 1 mM of IPTG was added to induce protein production from plasmids. After 4 h of induction, cells were fixed with 2.5% formaldehyde and 1.5% glutaraldehyde in 100 mM of sodium cacodylate buffer (pH 7.4) at 4°C for 12 h, followed by three washes with buffer alone for 5 min each wash. Cells were then fixed with 1% osmium tetroxide for 1 h in dark, followed by three washes with buffer. After treating the cells with 2% uranyl acetate in the dark for 1 h, cells were sequentially dehydrated in a graded ethanol series (50%, 70%, 85%, 95% and three times with 100% ethanol, for 5 min each), and three times with 100% acetone (5 min each). Dehydrated cells were embedded into epoxy resins for at least 12 h, and then sectioned into thin specimens (70 nm thick) using an ultramicrotome (UC6, Leica, Buffalo Grove, IL, USA). Specimens were stained with uranyl acetate and lead citrate, and

Table 2. Oligonucleotides used for site-directed mutagenesis (target mutated nucleotides are underlined), mutant construction and verification of kanamycin cassette insertion/removal (the homologous regions for the *ghoST* locus are double underlined).

Purpose/name	Sequence (5′ to 3′)
Site-directed mutagenesis	
ghoT-ATG-f	AAAGAGGAGAAATTAACTACGAGAGGATCTCACCAT
ghoT-ATG-r	ATGGTGAGATCCTCTCGTAGTTAATTTCTCCTCTTT
ghoT-GCA1-f	GATCCGGCCCTGAGGGCCGCCCTATTCTCTAAAATATT
ghoT-GCA1-r	AATATTTTAGAGAATAGGGCGGCCCTCAGGGCCGGATC
ghoT-GCA2-f	TCGTTTACTTAGTGCCTTCCTGGTCGGAATA
ghoT-GCA2-r	TATTCCGACCAGGAAGGCACTAAGTAAACGA
ghoT-GCA3-f	AATGAGTCTGCCTGTGGCCTTACTTTTTTCTCTCTTTGG
ghoT-GCA3-r	CCAAAGAGAGAAAAAAGTAAGGCCACAGGCAGACTCATT
ghoT-I21R-f	ATTCGTTTACTTAGTGCACGCCTGGTCGGAATAACCTGG
ghoT-I21R-r	CCAGGTTATTCCGACCAGGCGTGCACTAAGTAAACGAAT
ghoT-R38F-f	ATTCGTTTACTTAGTGCATTCCTGGTCGGAATAACCTGG
ghoT-R38F-r	CCAGGTTATTCCGACCAGGAATGCACTAAGTAAACGAAT
Mutant construction	
D*ghoST*fwd	GAGTACAGAGTCACGATATTTTTCATTCTCTCCGCGATGTTGTGTAGGCTGGAGCTGCTTC
D*ghoST*rev	GACGCTTCGTTTCACGATAACCAGCGGGTCCACTCAACCATGGTCCATATGAATATCCTCCTTAG
Verification of Kan insertion/removal	
C*ghoST*fwd2	AAGCCTGAAAGGGCAAGGGATTGGTAAAC
C*ghoST*rev2	GTCAGGCGACTGCTTCGTTCATCGTTC

f indicates forward primer, and r indicates reverse primer.

then examined on a FEI Tecnai G2 Spirit BioTwin TEM (Penn State Microscopy and Cytometry Facility, University Park, PA, USA) at an accelerating voltage of 120 kV.

Confocal fluorescence microscopy

Samples for fluorescence microscopy were prepared as described previously (Lamsa *et al*., 2012) with minor modifications. In brief, BW25113 and the Δ*ghoT* mutant were grown in LB medium overnight, washed twice with M9-Glu medium, diluted to turbidity at 600 nm of 0.05 in M9-Glu medium and grown for 8 h before harvest. Strains with plasmids were grown in LB with chloramphenicol (to maintain pCA24N derivatives) or kanamycin and erythromycin [to maintain both pBS(Kan) and pCM18 derivatives], diluted hundredfold in LB medium with antibiotics, grown until the turbidity at 600 nm reached 0.6–0.8, and induced with 1 mM of IPTG for 1 h. For microscopic observation, 1 ml of culture was centrifuged and resuspended in 100 μl M9-Glu or LB medium without antibiotics. For the treatment with nisin or CCCP, 1 ml of the NR698/pCA24N culture (OD_{600} = 0.6–0.8) was centrifuged, resuspended in 100 μl LB medium, and 14.25 or 13.5 μl was mixed with 0.75 μl of 10 mM CCCP, 1.5 μl of 0.5% DMSO or 1.5 μl 100 μg ml^{-1} nisin in a microcentrifuge tube for the incubation at 37°C for 1 h. Staining was performed by adding 6 μl of concentrated cells to 1.5 μl of a stain mix containing 30 μg ml^{-1} FM4–64, 2.5 μM SYTOX Green (omitted for pCM18-harboring cultures) and 1.2 μg ml^{-1} DAPI prepared in 1 × phosphate-buffered saline (PBS). The stained samples (7.5 μl) were immobilized on an agarose pad (1/10 × LB, 0.375 μg ml^{-1} FM4–64 and 0.025 μg ml^{-1} DAPI), and the images were taken using an Olympus FV1000 Laser Scanning Confocal Microscope on an IX-81 inverted microscope (Olympus America, Melville, NY, USA) at 1000× magnification. The medial focal planes were deconvolved using the FV10-ASW v3.0 software (Olympus).

ATP assay

The strains were grown as described above, induced with 1 mM of IPTG for 2 h and harvested by centrifugation. The cells were washed with 50 mM Tris-acetate (pH 7.75), and ATP was extracted by 1% trichloroacetic acid in 100 μl Tris-acetate buffer at 4°C for 10 min. One millilitre of Tris-acetate buffer was added to obtain a pH of 7.75, and cell debris was removed after centrifugation. Ten microlitre of the supernatant was then mixed with 100 μl rL/L reagent (ENLITEN ATP assay, Promega, Madison, WI, USA) pre-warmed at room temperature. Luminescence values were determined using a 5 s delay time and a 10 s relative light unit (RLU) signal integration time on a Turner TD-20e luminometer (Turner Designs, Sunnyvale, CA, USA). The amount of extracted ATP was calculated based on values determined using serial dilutions of known amounts of ATP for a standard curve following the manufacturer's recommendations. In each experimental sample, the RLU was divided by the turbidity at 600 nm to represent the levels of ATP in each culture. Values obtained from GhoT or GhoTF38R producing strains were divided by the value from BW25113/pCA24N to obtain the relative ATP levels. The ATP level in BW25113/pCA24N (25.13 ± 1.18 nmol g^{-1} cell) is around one third of the value reported in exponential-phased *E. coli* MG1655 (Buckstein *et al*., 2008) [25.5 nmol l^{-1}, or 85 nmol g^{-1} cell given that 1 OD_{600} = 0.3 g l^{-1} (Kim *et al*., 2012)].

PMF

The PMF was measured by flow cytometry as described previously (Lamsa *et al*., 2012). Strains were grown as described for fluorescence microscopy, and 6 μl of DMSO/CCCP-treated cells or the IPTG-induced cells was added to 1.5 μl of a stain mix containing 5 μg ml^{-1} $DiBAC_4(3)$ in 1 × PBS. The stained sample was added to 500 μl 1 × PBS, and 100 000 events were counted using a Fortessa LSR II

flow cytometer (BD, Franklin Lakes, NJ, USA). After the excitation by a 488 nm laser, the fluorescence data were collected using the 505 nm filter.

Lysis assay

To determine the level of cell lysis, β-galactosidase activity was measured and calculated as described previously (Ma and Wood, 2009). For checking cell lysis during the exponential phase, overnight cultures of BW25113 and the Δ*ghoT* mutant carrying pCA24N-*lacZ* grown in LB medium with chloramphenicol were washed twice with M9-Glu medium, resuspended and diluted in M9-Glu medium to turbidity of 0.05. Cells were grown for 4 h, then induced with 0.5 mM IPTG for 4 h and collected by centrifugation. For checking cell lysis during the stationary phase, the same strains were grown in M9-Glu medium for 20 h. For the positive control in which cell lysis was caused by overproducing GhoT, overnight cultures of MG1655/pCA24N-*ghoT* and MG1655/pCA24N were diluted into LB medium with chloramphenicol to a turbidity of 0.05, grown to a turbidity of 0.5 and induced with 1 mM IPTG for 10.5 h. The β-galactosidase activities were determined from both supernatants and cell pellets (the cell pellets were sonicated to release all of the cytosolic β-galactosidase), and the level of cell lysis was calculated from the percentage of the supernatant β-galactosidase activity in both the supernatant and cell pellets. Two independent samples were investigated ($n = 2$).

Western blot analysis

Overnight cultures of *E. coli* BW25113/pCA24N-*ghoT*-F38R were diluted 500-fold into 1 l of LB medium with chloramphenicol, grown to a turbidity of 1.0, induced with 0.1 mM of IPTG at room temperature overnight and collected by centrifugation at 8132 r.p.m. (for Beckman rotor JA-20) at 4°C. A 1 ml sample was taken out from the 1 l induced culture (to be used as a total cellular protein sample 'T'), the cell pellet mixed with 1× sodium dodecyl sulfate polyacrylamide gel electrophoresis sample loading buffer, and boiled at 95°C for 20 min before loading to the gel. Cells were broken by passing through a French press twice and centrifuged at 12858 r.p.m. (for Beckman rotor JA-20) for 60 min at 4°C. The insoluble protein from 1 l culture was extracted with 25 ml purification buffer (20 mM Tris-HCl, pH 7.9 and 500 mM NaCl) containing 6 N urea, and a sample was taken from the remaining insoluble fraction (sample 'I'). The supernatant was subjected to ultracentrifugation at 31170 r.p.m. (for Beckman rotor type 70 Ti) for 60 min at 4°C to separate the cytosolic (supernatant, sample 'C') and membrane proteins (pellet, sample 'M'). Western blot was performed as described previously (Wang *et al*., 2012), with ~20 μg of each protein sample and probed with primary antibodies raised against a His tag (Cell Signaling Technology, Danvers, MA, USA) and horseradish peroxidase-conjugated goat anti-mouse secondary antibodies (Fisher Scientific, Pittsburgh, PA, USA).

Phenotype microarrays and verification

A full phenotype array analysis (PM plates 1–20) was conducted by BioLog (Hayward, CA, USA). Two independent cultures were used for the initial screen of 1197 conditions, including 960 different nutrient conditions and 237 toxins (at four concentrations) for differences in metabolic activity. Four antimicrobials were identified, including cefoxitin, carbenicillin, 5,7-dichloro-8-hydroxyquinoline and 2-phenylphenol. The results were verified via six independent cultures using BioLog reagents by growing cells to a turbidity of 1.0, diluting to a turbidity of 0.07 in IF-10a (Cat. no. 72264) and then further diluting 200-fold into a reagent mixture containing IF-10a, BioLog Redox Dye D (Cat. no. 74224) and rich medium (2.0 g of tryptone, 1.0 g of yeast extract, and 1.0 g of NaCl per litre) to a final turbidity of 0.00035. This cell suspension (100 μl) was transferred into 96-well microtitre plates, incubated at 37°C, and the metabolic activity was monitored hourly by taking the absorbance (590 nm), which indicates the intracellular reducing state based on the generation of formazane (purple) from the tetrazolium dye.

Acknowledgements

This work was supported by the NIH (R01 GM089999). T. K. W. is the Biotechnology Endowed Professor at the Pennsylvania State University. We are grateful for the Keio and ASKA strains provided by the Genome Analysis Project in Japan, for the assistance provided by the Penn State Microscopy and Cytometry Facility and for the assistance of Brian Kwan with TEM.

References

Acebrón, S.P., Fernández-Sáiz, V., Taneva, S.G., Moro, F., and Muga, A. (2008) DnaJ recruits DnaK to protein aggregates. *J Biol Chem* **283:** 1381–1390.

Amitai, S., Kolodkin-Gal, I., Hananya-Meltabashi, M., Sacher, A., and Engelberg-Kulka, H. (2009) *Escherichia coli* MazF leads to the simultaneous selective synthesis of both 'death proteins' and 'survival proteins'. *PLoS Genet* **5:** e1000390.

Baba, T., Ara, T., Hasegawa, M., Takai, Y., Okumura, Y., Baba, M., *et al*. (2006) Construction of *Escherichia coli* K-12 in-frame, single-gene knockout mutants: the Keio collection. *Mol Syst Biol* **2:** 2006–2008.

Berney, M., Weilenmann, H.U., and Egli, T. (2006) Flow-cytometric study of vital cellular functions in *Escherichia coli* during solar disinfection (SODIS). *Microbiology* **152:** 1719–1729.

Blattner, F.R., Guy Plunkett, I., Bloch, C.A., Perna, N.T., Burland, V., Riley, M., *et al*. (1997) The complete genome sequence of *Escherichia coli* K-12. *Science* **277:** 1453–1462.

Bochner, B.R., Gadzinski, P., and Panomitros, E. (2001) Phenotype microarrays for high-throughput phenotypic testing and assay of gene function. *Genome Res* **11:** 1246–1255.

Buckstein, M.H., He, J., and Rubin, H. (2008) Characterization of nucleotide pools as a function of physiological state in *Escherichia coli*. *J Bacteriol* **190:** 718–726.

Canada, K.A., Iwashita, S., Shim, H., and Wood, T.K. (2002) Directed evolution of toluene *ortho*-monooxygenase for enhanced 1-naphthol synthesis and chlorinated ethene degradation. *J Bacteriol* **184:** 344–349.

Christensen, S.K., Mikkelsen, M., Pedersen, K., and Gerdes, K. (2001) RelE, a global inhibitor of translation, is activated during nutritional stress. *Proc Natl Acad Sci U S A* **98:** 14328–14333.

Christensen-Dalsgaard, M., and Gerdes, K. (2006) Two *higBA* loci in the *Vibrio cholerae* superintegron encode mRNA cleaving enzymes and can stabilize plasmids. *Mol Microbiol* **62:** 397–411.

Christensen-Dalsgaard, M., Jørgensen, M.G., and Gerdes, K. (2010) Three new RelE-homologous mRNA interferases of *Escherichia coli* differentially induced by environmental stresses. *Mol Microbiol* **75:** 333–348.

Datsenko, K.A., and Wanner, B.L. (2000) One-step inactivation of chromosomal genes in *Escherichia coli* K-12 using PCR products. *Proc Natl Acad Sci U S A* **97:** 6640–6645.

Dethlefsen, L., and Schmidt, T.M. (2007) Performance of the translational apparatus varies with the ecological strategies of bacteria. *J Bacteriol* **189:** 3237–3245.

Doyle, S.M., and Wickner, S. (2009) Hsp104 and ClpB: protein disaggregating machines. *Trends Biochem Sci* **34:** 40–48.

Dörr, T., Vulić, M., and Lewis, K. (2010) Ciprofloxacin causes persister formation by inducing the TisB toxin in *Escherichia coli*. *PLoS Biol* **8:** e1000317.

Edgar, R., Rokney, A., Feeney, M., Semsey, S., Kessel, M., Goldberg, M.B., *et al*. (2008) Bacteriophage infection is targeted to cellular poles. *Mol Microbiol* **68:** 1107–1116.

Engelberg-Kulka, H., Amitai, S., Kolodkin-Gal, I., and Hazan, R. (2006) Bacterial programmed cell death and multicellular behavior in bacteria. *PLoS Genet* **2:** e135.

Gerdes, K., Christensen, S.K., and Løbner-Olesen, A. (2005) Prokaryotic toxin-antitoxin stress response loci. *Nat Rev Microbiol* **3:** 371–382.

Hansen, M.C., Palmer, R.J., Jr, Udsen, C., White, D.C., and Molin, S. (2001) Assessment of GFP fluorescence in cells of *Streptococcus gordonii* under conditions of low pH and low oxygen concentration. *Microbiology* **147:** 1383–1391.

Hayes, F., and Van Melderen, L. (2011) Toxins-antitoxins: diversity, evolution and function. *Crit Rev Biochem Mol Biol* **46:** 386–408.

Hu, Y., Benedik, M.J., and Wood, T.K. (2012) Antitoxin DinJ influences the general stress response through transcript stabilizer CspE. *Environ Microbiol* **14:** 669–679.

Janowiak, B.E., Fischer, A., and Collier, R.J. (2010) Effects of introducing a single charged residue into the phenylalanine clamp of multimeric anthrax protective antigen. *J Biol Chem* **285:** 8130–8137.

Jayaraman, R. (2008) Bacterial persistence: some new insights into an old phenomenon. *J Biosci* **33:** 795–805.

Kelley, L.A., and Sternberg, M.J. (2009) Protein structure prediction on the web: a case study using the Phyre server. *Nat Protoc* **4:** 363–371.

Keren, I., Shah, D., Spoering, A., Kaldalu, N., and Lewis, K. (2004) Specialized persister cells and the mechanism of multidrug tolerance in *Escherichia coli*. *J Bacteriol* **186:** 8172–8180.

Khakimova, M., Ahlgren, H.G., Harrison, J.J., English, A.M., and Nguyen, D. (2013) The stringent response controls catalases in *Pseudomonas aeruginosa* and is required for hydrogen peroxide and antibiotic tolerance. *J Bacteriol* **195:** 2011–2020.

Kim, H.J., Kwon, Y.D., Lee, S.Y., and Kim, P. (2012) An engineered *Escherichia coli* having a high intracellular level of ATP and enhanced recombinant protein production. *Appl Microbiol Biotechnol* **94:** 1079–1086.

Kim, Y., and Wood, T.K. (2010) Toxins Hha and CspD and small RNA regulator Hfq are involved in persister cell formation through MqsR in *Escherichia coli*. *Biochem Biophys Res Commun* **391:** 209–213.

Kim, Y., Wang, X., Qun, M., Zhang, X.-S., and Wood, T.K. (2008) Toxin-antitoxin systems in *Escherichia coli* influence biofilm formation through YjgK (TabA) and fimbriae. *J Bacteriol* **191:** 1258–1267.

Kitagawa, M., Ara, T., Arifuzzaman, M., Ioka- Nakamichi, T., Inamoto, E., Toyonaga, H., and Mori, H. (2005) Complete set of ORF clones of *Escherichia coli* ASKA library (a complete set of *E. coli* K-12 ORF archive): unique resources for biological research. *DNA Res* **12:** 291–299.

Kolodkin-Gal, I., and Engelberg-Kulka, H. (2006) Induction of *Escherichia coli* chromosomal *mazEF* by stressful conditions causes an irreversible loss of viability. *J Bacteriol* **188:** 3420–3423.

Kolter, R. (2010) Biofilms in lab and nature: a molecular geneticist's voyage to microbial ecology. *Int Microbiol* **13:** 1–7.

Krantz, B.A., Melnyk, R.A., Zhang, S., Juris, S.J., Lacy, D.B., Wu, Z., *et al*. (2005) A phenylalanine clamp catalyzes protein translocation through the anthrax toxin pore. *Science* **309:** 777–781.

Kwan, B.W., Valenta, J.A., Benedik, M.J., and Wood, T.K. (2013) Arrested protein synthesis increases antibiotic persistence. *Antimicrob Agents Chemother* **57:** 1468–1473.

Lamsa, A., Liu, W.T., Dorrestein, P.C., and Pogliano, K. (2012) The *Bacillus subtilis* cannibalism toxin SDP collapses the proton motive force and induces autolysis. *Mol Microbiol* **84:** 486–500.

Lewis, K. (2007) Persister cells, dormancy and infectious disease. *Nat Rev Microbiol* **5:** 48–56.

Li, G., and Young, K.D. (2012) Isolation and identification of new inner membrane-associated proteins that localize to cell poles in *Escherichia coli*. *Mol Microbiol* **84:** 276–295.

Liu, W.T., Yang, Y.L., Xu, Y., Lamsa, A., Haste, N.M., Yang, J.Y., *et al*. (2010) Imaging mass spectrometry of intraspecies metabolic exchange revealed the cannibalistic factors of *Bacillus subtilis*. *Proc Natl Acad Sci U S A* **107:** 16286–16290.

Ma, Q., and Wood, T.K. (2009) OmpA influences *Escherichia coli* biofilm formation by repressing cellulose production through the CpxRA two-component system. *Environ Microbiol* **11:** 2735–2746.

Maisonneuve, E., Shakespeare, L.J., Jørgensen, M.G., and Gerdes, K. (2011) Bacterial persistence by RNA endonucleases. *Proc Natl Acad Sci U S A* **108:** 13206–13211.

Masuda, H., Tan, Q., Awano, N., Wu, K.P., and Inouye, M. (2012) YeeU enhances the bundling of cytoskeletal polymers of MreB and FtsZ, antagonizing the CbtA (YeeV) toxicity in *Escherichia coli*. *Mol Microbiol* **84:** 979–989.

Nguyen, D., Joshi-Datar, A., Lepine, F., Bauerle, E., Olakanmi, O., Beer, K., *et al*. (2011) Active starvation responses mediate antibiotic tolerance in biofilms and nutrient-limited bacteria. *Science* **334:** 982–986.

Pecota, D.C., and Wood, T.K. (1996) Exclusion of T4 phage by the *hok/sok* killer locus from plasmid R1. *J Bacteriol* **178:** 2044–2050.

Prasad, I., and Schaefler, S. (1974) Regulation of the β-glucoside system in *Escherchia coli* K-12. *J Bacteriol* **120:** 638–650.

Ren, D., Bedzyk, L.A., Thomas, S.M., Ye, R.W., and Wood, T.K. (2004) Gene expression in *Escherichia coli* biofilms. *Appl Microbiol Biotechnol* **64:** 515–524.

Rokney, A., Shagan, M., Kessel, M., Smith, Y., Rosenshine, I., and Oppenheim, A.B. (2009) *E. coli* transports aggregated proteins to the poles by a specific and energy-dependent process. *J Mol Biol* **392:** 589–601.

Romantsov, T., Helbig, S., Culham, D.E., Gill, C., Stalker, L., and Wood, J.M. (2007) Cardiolipin promotes polar localization of osmosensory transporter ProP in *Escherichia coli*. *Mol Microbiol* **64:** 1455–1465.

Ruiz, N., Falcone, B., Kahne, D., and Silhavy, T.J. (2005) Chemical conditionality: a genetic strategy to probe organelle assembly. *Cell* **121:** 307–317.

Sampson, B.A., Misra, R., and Benson, S.A. (1989) Identification and characterization of a new gene of *Escherichia coli* K-12 involved in outer membrane permeability. *Genetics* **122:** 491–501.

Sourjik, V., and Berg, H.C. (2000) Localization of components of the chemotaxis machinery of *Escherichia coli* using fluorescent protein fusions. *Mol Microbiol* **37:** 740–751.

Tan, Q., Awano, N., and Inouye, M. (2011) YeeV is an *Escherichia coli* toxin that inhibits cell division by targeting the cytoskeleton proteins, FtsZ and MreB. *Mol Microbiol* **79:** 109–118.

The UniProt Consortium (2012) Reorganizing the protein space at the Universal Protein Resource (UniProt). *Nucleic Acids Res* **40:** D71–D75.

Unoson, C., and Wagner, E.G. (2008) A small SOS-induced toxin is targeted against the inner membrane in *Escherichia coli*. *Mol Microbiol* **70:** 258–270.

Wang, X., and Wood, T.K. (2011) Toxin/antitoxin systems influence biofilm and persister cell formation and the general stress response. *Appl Environ Microbiol* **77:** 5577–5583.

Wang, X., Kim, Y., Hong, S.H., Ma, Q., Brown, B.L., Pu, M., *et al*. (2011) Antitoxin MqsA helps mediate the bacterial general stress response. *Nat Chem Biol* **7:** 359–366.

Wang, X., Lord, D.M., Cheng, H.-Y., Osbourne, D.O., Hong, S.H., Sanchez-Torres, V., *et al*. (2012) A new type V toxin-antitoxin system where mRNA for toxin GhoT is cleaved by antitoxin GhoS. *Nat Chem Biol* **8:** 858–861.

Wang, X., Lord, D.M., Hong, S.H., Peti, W., Benedik, M.J., Page, R., and Wood, T.K. (2013) Type II toxin/antitoxin MqsR/MqsA controls type V toxin/antitoxin GhoT/GhoS. *Environ Microbiol* **15:** 1734–1744.

Winkler, J., Seybert, A., König, L., Pruggnaller, S., Haselmann, U., Sourjik, V., *et al*. (2010) Quantitative and spatio-temporal features of protein aggregation in *Escherichia coli* and consequences on protein quality control and cellular ageing. *EMBO J* **29:** 910–923.

Wu, G., Wu, H., Fan, X., Zhao, R., Li, X., Wang, S., *et al*. (2010) Selective toxicity of antimicrobial peptide S-thanatin on bacteria. *Peptides* **31:** 1669–1673.

Wu, L.J., and Errington, J. (2003) RacA and the Soj-Spo0J system combine to effect polar chromosome segregation in sporulating *Bacillus subtilis*. *Mol Microbiol* **49:** 1463–1475.

Yamaguchi, Y., Park, J.-H., and Inouye, M. (2009) MqsR, a crucial regulator for quorum sensing and biofilm formation, is a GCU-specific mRNA interferase in *Escherichia coli*. *J Biol Chem* **284:** 28746–28753.